Potential Energy Surface for Asymmetrically Substituted Reactions of Type CWXYZ + A. Kinetics Study

Cipriano Rangel and Joaquín Espinosa-García*

Departamento de Química Física, Universidad de Extremadura, 06071 Badajoz, Spain

Received: February 14, 2007; In Final Form: March 30, 2007

The $CHClF_2 + Cl \rightarrow ClH + CClF_2$ gas-phase abstraction reaction was chosen as a model of asymmetrically substituted polyatomic reactions of type CWXYZ + A → products. The analytical potential energy surface for this reaction was constructed with suitable functional forms to represent vibrational modes, and calibrated with respect to experimental thermal rate constants which are available over the temperature range 296−410 K. On this surface, the thermal rate constants were calculated using variational transition-state theory with semiclassical transmission coefficients over a wider temperature range, 200−2500 K, therefore obtaining kinetics information at lower and higher temperatures than are experimentally available. This surface was also used to analyze dynamical features, such as tunneling and reaction-path curvature. In the former, the influence of the tunneling factor was important since a light hydrogen atom passes through the barrier. In the latter, it was found that vibrational excitation of the C−F and C−Cl stretching modes can be expected in the exit channel.

I. Introduction

Basically, three strategies for the construction of potential energy surfaces (PES) can be considered. Two are based on performing thousands of electronic structure calculations on different geometrical configurations, followed by either interpolation (global or local) or a fit to a suitable functional form. The third is based on choosing a suitable functional form and calibration against theoretical and/or experimental information. The first two strategies give adequate PESs only when very high level ab initio calculations (basis set and correlation energy) are used, which is still today prohibitive for atoms beyond the second row, and the computational cost increases exponentially with molecular size. The third strategy, although semiempirical, represents an economic, useful, and less time-consuming alternative.

Until now we had applied this economic alternative[1−8] to gas-phase symmetrically substituted polyatomic reactions of type $BX_n + A \rightarrow AX + BX_{n-1}$, where B is the central atom, A is the abstractor atom, and all the X substituents are equivalent. This equivalent character of the B−X bonds and X−B−X angles allowed a simplification of the problem, because all the bonds and angles were treated in the same way. Recently, our group[9] extended this strategy to gas-phase asymmetrically substituted polyatomic reactions, beginning with the simplest case, monosubstitution, i.e., only two different substituents on the central atom, $BYX_m + A$. This abstraction reaction can proceed through two reaction channels, $AX + BYX_{m-1}$, and $AY + BX_m$, which complicates the PES construction because now the bonds and angles must be treated independently.

The main goal of the present paper is to extend this method to asymmetrically poly substituted reactions of type BWXYZ + A, where all the bonds and angles must be independently treated. Clearly, the formulation of the functional forms, the compilation, and finally the calibration process will considerably increase in difficulty with respect to the symmetrically substituted reactions.

Unfortunately, experimental studies on these asymmetrically substituted reactions are scarce, and to test the strategy we shall build the PES for the gas-phase $CHClF_2 + Cl$ abstraction reaction, where the central atom is the carbon, and the abstractor atom is the chlorine, which a priori could proceed through three reaction channels: hydrogen, chlorine, and fluorine abstraction. While the two last channels are very endothermic,[10] +24.91 and +59.09 kcal mol^{-1}, respectively, and therefore disfavored, the first is energetically favored ($\Delta H_r^\circ = -0.05$ kcal mol^{-1}), so that we shall take it as the focus of the present study.

This reaction presents several important features that invite theoretical study. First, the study of hydrochlorofluorocarbons (HCFCs) is of great importance in atmospheric and combustion processes. Second, the experimental rate constants[15−18] are usually restricted to room temperature and show a broad range of values, although recent critical reviews[19−22] give a narrower range. Third, the theoretical studies on this reaction have also been scarce,[23−25] and a complete potential energy surface has not been constructed.

The article is structured as follow: In Section II we briefly outline the potential energy surface and the computational details. The results are presented in Section III, and compared with experiments and other theoretical results. Finally, Section IV presents the conclusions.

II. Potential Energy Surface and Computational Details

II.1. Functional Form. On the basis of our previous experience with symmetrically ($BX_4 + A$) and asymmetrically ($BX_3Y + A$) monosubstituted reactions, the new surface for poly substituted reactions of type BWXYZ + A, where W, X, Y, and Z can be equal or different, is formulated in similar terms,

* Corresponding author. E-mail: joaquin@unex.es.

10.1021/jp071264b CCC: $37.00
Published on Web 05/19/2007

i.e., stretching (str), valence (val) bending, and out-of-plane (op) bending, and has the general form

$$V = V_{str} + V_{val} + V_{op} \quad (1)$$

where V_{str} is the stretching term given by

$$V_{str} = V_3(R_{BW},R_{BA},R_{AW}) + V_3(R_{BX},R_{BA},R_{AX}) + V_3(R_{BY},R_{BA},R_{AY}) + + V_3(R_{BZ},R_{BA},R_{AZ}) \quad (2)$$

with W, X, Y, and Z being the possible abstracted atoms, A the abstractor, and V_3 represents the London−Eyring−Polanyi (LEP) functional form. Each V_3 term involves a singlet curve depending on three adjustable parameters ($^1D_{U-V}$, α_{U-V}, and $R_{U-V}{}^0$) and a triplet curve depending on three parameters ($^3D_{U-V}$, α_{U-V}, and $R_{U-V}{}^0$) for each U−V bond. The B−U (U = W, X, Y, Z) Morse parameters, α_{B-U}, are allowed to relax using a switching function, from reactant, BWXYZ, to products, depending on the pathway chosen

$$\alpha_{U-V} = a_{U-V} + b_{U-V}\left(\frac{\tanh[c_{U-V}(R - R^0)] + 1}{2}\right) \quad (3)$$

where R is the B−U bond length in the system, R^0 the corresponding equilibrium B−U bond length in the reactant, and a_{U-V}, b_{U-V}, and c_{U-V} are adjustable parameters to obtain accurate stretching frequencies at the reactants, products, and saddle point. This separation of the B−U stretching modes greatly complicates the calibration process because more parameters are involved, but permits us to separate all the possible abstraction channels using the same functional form. Note that in this case we have made a separation of the V_3 terms, and have the possibility of selecting all the reaction types (BW_4, BW_3X, BW_2X_2, BW_2XY, and BWXYZ) and all the channels in each type using the same functional form.

V_{val} is an harmonic term for valence bending:

$$V_{val} = \frac{1}{2}\sum_{i=1}^{3}\sum_{j=i+1}^{3} k_{ij}^0 k_i k_j (\theta_{ij} - \theta_{ij}^0)^2 \quad (4)$$

where the sum is over all the three atoms' possibilities i−B−j where i and j are the atoms bound to the center atom. The force constant, k_{ij}^0, is a function depending on adjustable parameters, and on the distances B−i and B−j, so we obtain the constant force independently, depending on which i and j atoms we are considering (k_{WX}^0, k_{WY}^0, k_{WZ}^0, k_{XY}^0, k_{XZ}^0, and k_{YZ}^0) and the reference angle θ_{ij}^0 represents the angle defined by two bonds (B-i, B-j) where i and j are W, X, Y, and Z. The k_{ij}^0 are also allowed to relax using a switching function from the reactant to product structure depending on the pathway chosen. As in the case of the V_{str} term, we made a separation of the V_{val} term between the i−B−j possibilities.

Finally, V_{op} is the out-of-plane bending term, correlating with the out-of-plane motion of the product radical in all the four possible pathways. Again we separated the distinct pathways that we can choose, and the expression is

$$V_{op} = \sum_{i=1}^{4} f_{\Delta i} \sum_{j=1,j\neq i}^{4} \Delta_{ij}{}^2 + \sum_{i=1}^{4} h_{\Delta i} \sum_{j=1,j\neq i}^{4} \Delta_{ij}{}^4 \quad (5)$$

The functional form is based on symmetric terms suggested by Duchovic et al.,[26] where

$$f_{\Delta i} = ([1 - S_3(R_i)]\cdot S_3(R_j)\cdot S_3(R_k)\cdot S_3(R_l)\cdot f_{\Delta}^{Bjkl}$$

$$h_{\Delta i} = ([1 - S_3(R_i)]\cdot S_3(R_j)\cdot S_3(R_k)\cdot S_3(R_l)\cdot h_{\Delta}^{Bjkl}$$

$$S_3(R) = 1 - \tanh[\alpha_3(R - R^0)(R - \beta_3)^2] \quad (6)$$

R being each of the B−U bonds (U = W, X, Y, and Z) and R^0 the corresponding equilibrium value, $f_{\Delta}{}^{Bjkl}$ and $h_{\Delta}{}^{Bjkl}$ being force constants for every possible *Bjkl* product, and

$$\Delta_{ij} = \cos^{-1}\left[\frac{(r_k - r_j)\times(r_l - r_j)}{||(r_k - r_j)\times(r_l - r_j)||}\cdot\frac{r_i}{||r_i||}\right] - \phi_{ij}^0 \quad (7)$$

where the vector $\mathbf{r}$ is associated with the bond R ($\mathbf{r}_{BW}$, $\mathbf{r}_{BX}$, $\mathbf{r}_{BY}$, and $\mathbf{r}_{BZ}$).

In sum, in this new PES we have separated the functional forms for each bond and angle, and have introduced 30 new (in total, 64) calibration parameters describing the behavior of the different atoms. Note that, as in the case of our previous PESs, this new PES is also symmetric with respect to the permutation of equivalent atoms in systems of type BW_2X_2 and BW_3X, a very important feature in dynamics studies. Therefore, to clarify the nomenclature, it is necessary to note that until now we had constructed PESs to describe symmetrically substituted reactions of type $BX_4 + A \rightarrow AX + BX_3$, and asymmetrically monosubstituted reactions of type $BX_3Y + A \rightarrow BX_3 + AY$ or $BX_2Y + AX$. Now with this work, we are introducing all the possible poly-substituted reactions of type BWXYZ + A → products, where W, X, Y, and Z can be equal or different (BW_4, BW_3X, BW_2X_2, BW_2XY, and BWXYZ), and opening all the possible paths for every reaction using the same functional form.

II.2. Calibration Process. Having selected the functional form, we next consider the calibration of the PES for the $CHClF2 + Cl \rightarrow ClH + CClF_2$ hydrogen abstraction reaction. This calibration process has been described in detail elsewhere,[1−9] and we shall present here just a short description of the process, although in this case, due to the independent treatment of the different bonds and angles, 64 parameters are involved, and the computational time and effort have considerably increased. The calibration process consists of three steps. In the first step, we changed the parameters $R_{U-V}{}^0$, $^1D_{U-V}$, and α_{U-V} for the different bonds in the system (C−H, C−Cl, and C−F in the CHF_2Cl molecule, and C−Cl with the abstractor atom) related to the geometric, energy, and vibrational properties of the reactants and products, so that the geometries, heat of reaction, and vibrational frequencies agree with the available experimental and/or theoretical data. In the second step, we refit the parameters $^3D_{U-V}$ for all the U−V bonds in the PES in order to reproduce the characteristics of the ab initio calculated saddle point, in particular, geometry, barrier height, and vibrational frequencies. During this fitting process, we took especial care to ensure that no artificially deep wells were introduced in the reactant or product valley. Note that the topology of the reaction path is very sensitive to the $^3D_{U-V}$ parameters, i.e., small changes in them produce large changes in the shape of the path, barrier height, and imaginary frequency. Finally, since a main objective in this work was to analyze dynamical details of the rate process (importance of tunneling, temperature dependence, possible vibrational excitation in reactants or products, etc.), as the third step of our calibration, we refit some of the parameters of the analytical PES (mainly the force constants, k_i, in the valence bending term, V_{val}, and the $f_{\Delta i}$ and $h_{\Delta i}$ parameters in the out-of-plane term, V_{op}), in order to reproduce the experi-

TABLE 1: Reactant and Product Properties[a] Calculated Using the Analytical Surface

	CHClF2		HC		CClF2	
	PES	exp.[b]	PES	exp.[b]	PES	theor.[c]
			Geometry			
d(C−H)	1.085	1.09				
d(C−F1)	1.297	1.35			1.322	1.31
d(C−F2)	1.320	1.35			1.322	1.31
d(C−Cl)	1.718	1.75			1.764	1.73
d(Cl−H)			1.234	1.28		
∠F−C−F	109.3				115.5	
∠F−C−Cl	110.7				115.5	113.7
∠H−C−Cl	109.7	107.0				
∠F−C−F−Cl					138.9	
			Frequency			
	3158	3035	2901	2991	1244	1251
	1573	1350			1222	1164
	1557	1310			716	768
	1215	1088			429	570
	1154	805			362	409
	873	794			349	352
	503	576				
	403	400				
	348	355				
ZPE	15.42	14.00	4.14	4.31	6.18	6.50
			Energy			
				ΔE_r	ΔH_r(0 K)	ΔH_r(298 K)
exp.						−0.05 ± 3.0[d]
UMP2/6-311G(2d,2p)[e]				3.53	−0.57	
UMP2/aug-cc-pvdz[e]				4.45	0.52	
QCISD(T)/6-311+G(d,p)[e]				5.70	1.77	
BH&HLYP/6-311G(d,p)[e]				5.76	1.54	
BH&HLYP/aug-cc-pvtz[e]				3.95	−0.18	
MP2/cc-VDZ[f]				4.76		
MP2/cc-VTZ[f]				2.60		
PES[f]				4.36	−0.73	

[a] Distances in Å, frequencies in cm^{-1}, energies in kcal mol^{-1}. [b] From ref 11. [c] From ref 23. [d] ΔHr (298 k) from the following enthalpies of formation: CHClF2, −115.3 ± 3.0 (ref 11); Cl, 28.99 (ref 11); ClH, −22.06 (ref 11); CClF2, −64.30 (ref 12), in kcal/mol. [e] From ref 25. [f] This work.

mental rate constants. Note that since this calibration is carried out by hand, the fitting performed in last steps obliges us to refit some of the parameters obtained in previous steps. This iterative process is tedious, non-trivial, and has to be followed until convergence with the experimental information.

Although more information on the topology of the reaction could help in this fitting process, our previous experience with similar potential energy surfaces indicated to us that the data set (reactant, products, and saddle-point properties and experimental rate constants) used here in the calibration process is adequate. Moreover, in this polyatomic system with several heavy atoms, the use of very high ab initio calculations to build the PES is practically prohibitive, and so our strategy using experimental rate constants in the calibration process, although semiempirical, is justified, useful, and economical. The final functional form and the adjustable parameters of the new PES are given on our Web page.[27]

As was noted in the Introduction, the experimental data on asymmetrically substituted reactions is scarce, and the present study is focused on the hydrogen abstraction. However, at this point it is necessary to take into account that in the general case of a multichannel reaction the same functional form is used for all the channels, the difference being in the calibration process exclusively. Therefore, if three channels are possible, three independent calibration processes are necessary on the same functional form. This was the approach used in an earlier study[9] on the asymmetrically monosubstituted $H+CH_3Cl$ reaction, which proceeds through two channels, CH_3+ClH, and CH_2Cl+H_2. There, we performed two independent calibrations using the same functional form.

The results of the final fit are listed in Table 1 for reactants and products, and in Table 2 for the saddle point. In general, the reactant and product properties agree with the experimental data,[11,12] with an enthalpy of reaction at 0 K of −0.73 kcal mol^{-1}, versus the experimental value of −0.05 ± 3.00 kcal mol^{-1} (value at 298 K, because the enthalpies of formation are available only at this temperature for all components). This agreement is, obviously, a consequence of the fitting procedure used, and represents simply a check of the consistency of the parametrization. Next we consider the properties of the saddle point, especially the barrier height (Table 2). It is well-known that the classical barrier height ($\Delta E^{\ddagger}$) is very sensitive to the method used (correlation energy and basis set), a general problem in computational chemistry. The theoretical (ab initio and DFT) calculations (ref 25 and this work) used as initial reference give barriers in a wide range, 9.55−12.89 kcal mol^{-1}, and an average value (about 11 kcal mol^{-1}) was chosen for the calibration. When the ZPE correction is included, our V_a^G value, 4.01 kcal mol^{-1}, is lower than other ab initio calculations by about 1 kcal mol^{-1}, with the largest difference being with calculations at the QCISD(T)/6-311+G(2d,2p) level, possibly due to the limited basis set used at this level. The saddle-point geometry shows reasonable agreement with the sparse ab initio and DFT quantum chemical calculations, although the new surface has a shorter Cl−H′ bond. The transition state is "late", i.e., a product-like transition state, where the length of the bond

TABLE 2: Saddle-Point Properties[a]

	CHClF2-Cl		
	PES	theor.[b]	MP2/cc-VTZ[d]
	Geometry		
d(C−H)	1.31	1.38	1.28
d(C−F_1)	1.30	1.30	1.32
d(C−F_2)	1.33	1.30	1.32
d(C−Cl)	1.76	1.73	1.73
d(Cl−H)	1.28	1.46	1.50
∠F−C−F	112.0		
∠H−C−Cl	102.4	106.7	
	Frequency		
	1243	1320	
	1183	1234	
	824	1020	
	716	1015	
	713	910	
	474	672	
	383	453	
	346	386	
	262	178	
	66	113	
	54	91	
	1387i	1332i	
ZPE Energy	8.95	10.57	

	$\Delta E^{\neq}$	$\Delta H^{\neq}$ (0 K)
UMP2/6-311G(2d,2p)[c]	9.76	5.33
UMP2/aug-cc-pvdz[c]	9.86	5.54
QCISD/6-311+G(2d,2p)[c]	10.10	5.53
QCISD(T)/6-311+G(2d,2p)[c]	12.79	8.21
BH&HLYP/6-311 G(d,p)[c]	12.07	7.38
BH&HLYP/aug-cc-pvtz[c]	11.49	6.88
MP2/cc-VDZ[d]	11.57	
MP2/cc-VTZ[d]	9.55	
PES	10.71	4.01

[a] Distances in Å, frequencies in cm^{-1}, energies in kcal mol^{-1}. [b] Ref 23. [c] Ref 25. [d] This work.

that is broken (C−H′) increases by 21%, and the length of the bond that is formed (Cl−H′) is 4% larger than at the products.

II.3. Computational Details. With the new surface calibrated as described in the previous section, the saddle point was identified by having one negative eigenvalue of the Hessian matrix, and therefore one imaginary frequency. Starting from the saddle point, we followed the reaction-path in mass-weighted Cartesian coordinates, obtaining the minimum energy path (MEP).[28] Along the MEP, we calculated vibrational frequencies after projecting out the motion along the reaction-path using redundant internal coordinates.[29] With this information, we calculated first the vibrationally adiabatic ground-state potential (V_a^G) that can be considered as the free energy along the reaction-path at 0 K, and second the coupling terms,[30] $B_{k,F}(s)$, measuring the coupling between the normal mode, k, and the motion along the reaction coordinate (s), mode F. These coupling terms control the nonadiabatic flow of energy between these modes and the reaction coordinate,[31,32] and are the components of the reaction path curvature, $\kappa(s)$, defined as

$$\kappa(s) = (\Sigma[B_k,F(s)]^2)^{1/2} \quad (8)$$

Rate constants were estimated using canonical variational transition-state theory (CVT).[33] Quantum effects on motions transversal to the reaction-path were included using quantum-mechanical vibrational partition functions under the harmonic oscillator approach, while quantum effects in the motion along the reaction-path were included using the microcanonical optimized multidimensional tunneling (μOMT) method, in which (at each energy) the transmission probability is taken as the maximum of two trial calculations, namely, the small-curvature tunneling (SCT)[34] and the large-curvature tunneling (LCT)[35] methods. The analysis of the V_a^G curve showed the existence of two maxima and, therefore, the rate constants were finally calculated using the canonical unified statistical (CUS) model.[33,36]

All dynamical calculations were performed using the general polyatomic rate constants code POLYRATE.[37]

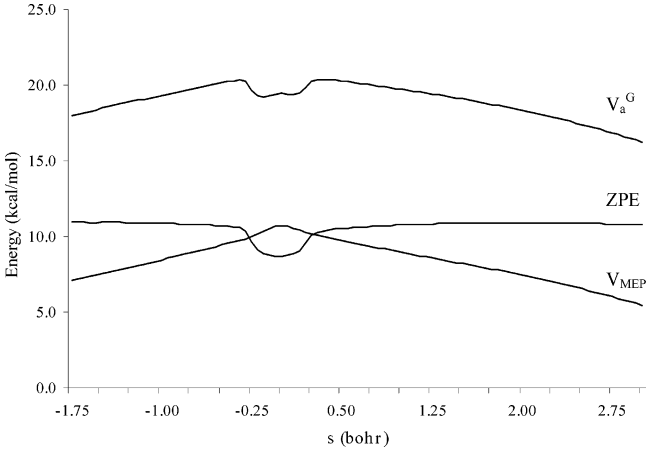

Figure 1. Classical potential energy curve, V_{MEP}, zero-point energy curve, ZPE, and vibrationally adiabatic potential energy curve, V_a^G, as functions of the reaction coordinate s.

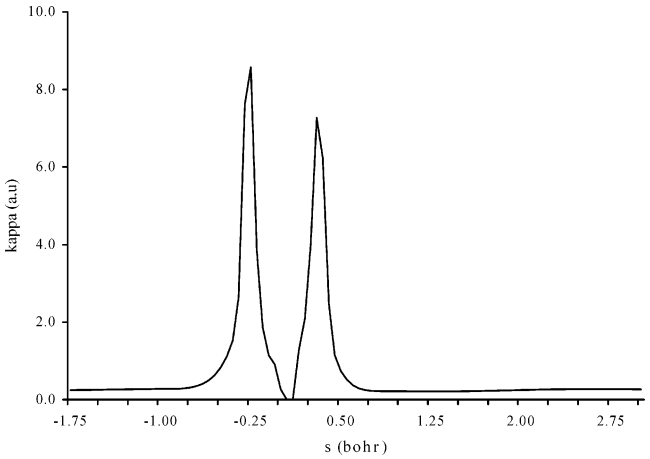

Figure 2. Reaction path curvature κ(s) as a function of s.

III. Results and Discussion

III.1. Reaction Path and Curvature Terms. Figure 1 shows the classical potential energy, V_{MEP}, the ground-state vibrationally adiabatic potential energy, V_a^G, and the local zero-point energy, ZPE, as a function of s over the range −2.0 to +3.0 bohr.

The ZPE curve drops in the saddle-point zone, showing a broad well. This behavior is typical of hydrogen abstraction reactions, and the change with s is mainly due to the drop in the C−H stretching corresponding to the normal mode breaking during the reaction, which evolves to the Cl−H stretching mode forming in the product (reactive mode). As a consequence, the V_a^G curve presents a deep well, with two maxima.

Along the MEP the coupling terms, $B_{k,F}(s)$, between the reaction coordinate and the orthogonal bound modes control the non-adiabatic flow of energy between these modes and the reaction coordinate. Figure 2 shows the reaction path curvature (κ) as a function of s. There are two sharp peaks, one on the

TABLE 3: Variational Rate Constants and Tunneling Transmission Coefficients (κ) Obtained with This PES, Together with the Experimental Values for Comparison

T (K)	TST	CVT	CUS	SCT	LCT	CUS/μ-OMT	exp.[a]
200	1.50×10^{-16}	1.30×10^{-17}	7.26×10^{-18}	1.88	3.77	2.74×10^{-17}	
300	9.27×10^{-15}	1.69×10^{-15}	9.74×10^{-16}	1.34	1.97	1.91×10^{-15}	1.40×10^{-15},[b] 1.69×10^{-15},[c] 2.01×10^{-15},[d] 1.91×10^{-15}[e]
400	9.63×10^{-14}	2.45×10^{-14}	1.46×10^{-14}	1.18	1.50	2.18×10^{-14}	
700	3.80×10^{-12}	1.33×10^{-12}	8.33×10^{-13}	1.06	1.15	9.56×10^{-13}	
900	1.50×10^{-11}	5.51×10^{-12}	3.48×10^{-12}	1.03	1.09	3.78×10^{-12}	
1000	2.55×10^{-11}	9.49×10^{-12}	5.99×10^{-12}	1.03	1.07	6.40×10^{-12}	
2000	4.88×10^{-10}	1.81×10^{-10}	1.12×10^{-10}	1.01	1.02	1.14×10^{-10}	
2500	1.05×10^{-9}	3.86×10^{-10}	2.37×10^{-10}	1.00	1.01	2.39×10^{-10}	

[a] Experimental values at 298 K. [b] Ref 15. [c] Ref 17. [d] Ref 16. [e] Refs 19 and 21.

reactant side, which has a value of 8.57 au at $s = -0.25$ bohr, and one on the product side, which has a value of 7.27 au at $s = +0.40$ bohr. The first is due to strong coupling of the reaction path to all stretching modes in the $CHClF_2$ reactant. Excitation of these modes might be expected to enhance the forward reaction rates. The second is in the exit channel and is lower than the first. It is due to the coupling of the reaction path to the C−F, C−Cl, and Cl−H stretching modes. This might be an indication that these modes in the products for the forward reaction could appear vibrationally excited. However, if one examines the V_a^G curve (Figure 1), one notes that the energy difference between the maximum of the V_a^G and the products is 5.71 kcal mol^{-1}, and therefore there is not enough available energy to excite by one quantum the Cl−H stretch mode (2901 cm^{-1} ≈ 8.3 kcal mol^{-1}) if the system passes through the transition state region in the ground vibrational state, although there is enough energy to excite by one quantum the C−F and C−Cl stretching modes (1243 cm^{-1} ≈ 3.6 kcal mol^{-1}, and 1222 cm^{-1} ≈ 3.5 kcal mol^{-1}, respectively). Therefore, for the thermal forward reaction the Cl−H stretch mode will appear vibrationally unexcited, while the C−F and C−Cl modes can appear vibrationally excited.

III.2. Thermal Rate Constants. In variational transition-state theory, the location of the dividing surface is varied along the reaction-path to minimize the rate constants, obtaining the canonical variational transition-state. The location of the dynamic bottleneck of the thermally averaged reaction shows little dependence on this optimization, ranging from 0.325 bohr at 0 K to 0.302 bohr at 2500 K. The variational effects (i.e., the ratio between variational CVT and conventional TST rate constants) change from 0.086 at 200 K to 0.367 at 2500 K. For this reaction, the energy contribution (high barrier height) dominates over the entropy contribution, even at high temperatures.

Table 3 lists the variational rate constants and the tunneling transmission coefficients (κ) obtained with this PES, together with the experimental values for comparison, and Figure 3 shows the corresponding Arrhenius plots. The CUS/μOMT rate constants agree with experiment[18] and recent reviews[19−22] in the common temperature range (296−410 K). However, as was indicated in Section II, as the experimental rate constants were used in the calibration process of the new PES, this agreement simply represents a check on the consistency of the parametrization. The DFT calculations of Xiao et al.[23] and Li and Wang[24] underestimate the experimental values, while the agreement found by Knyazev[25] using a modest TST-Eckart based model is only a consequence of the fitting procedure used to reproduce the experimental information.

Moreover, the new PES has a novel kinetics usefulness: the extrapolation of rate constants to higher ($T > 500$ K) and lower ($T < 300$ K) temperatures, which are not available experimentally, and have therefore not been used in the calibration process. These higher and lower temperature ranges are of interest in combustion and atmospheric chemistry, respectively.

With respect to the tunneling effect (Table 3), the use of an analytical PES permits one to use the LCT approach, which was not possible in earlier theoretical works,[23,24] which used the SCT method. These different approaches have a great influence on the final results, especially at low temperatures. For instance, at 200 K, while the SCT transmission coefficient is 1.88, the LCT approach gives 3.77; i.e., the rate constant is increased by a factor of 2.0. This behavior was to be expected, since the abstraction reaction involves the motion of a light particle (a hydrogen atom) that can easily tunnel through the reaction barrier.

Finally, the activation energy can be obtained by determining the slope of the Arrhenius plot. In the common temperature range (296−410 K), our activation energy, 5.8 kcal mol^{-1}, is close to the experimental value[18] of 4.8 ± 0.2 kcal mol^{-1}.

IV. Conclusions

In this work we have extended the knowledge of the construction of analytical potential energy surfaces for polyatomic systems to asymmetrically substituted reactions of type BWXYZ +A, where A is the abstractor atom. Here we constructed the analytical PES for the $CHClF_2 + Cl \rightarrow ClH + CClF_2$ gas-phase hydrogen abstraction reaction based on a suitable functional form, and using as calibration criterion the fit to the available experimental thermal rate constants. For this polyatomic system the functional forms were separated for each bond and angle, introducing 30 new calibration parameters with respect to the previous symmetrically substituted systems. This meant that there are 64 parameters in total, which represents the greatest challenge.

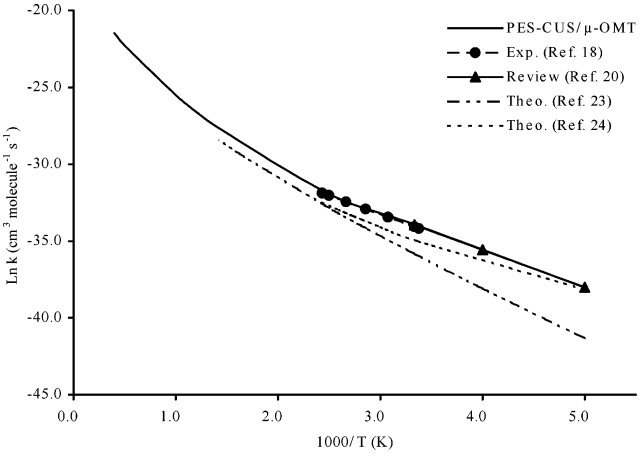

Figure 3. Arrhenius plot of ln k (cm^3 molecule^{-1} s^{-1}) against the reciprocal of the temperature (K) for the forward thermal reaction together with the experimental and other theoretical values for comparison.

The agreement with the experimental rate constants in the common temperature range (296−410 K) is of course just a consequence of the parametrization used, but first it does lend confidence to the new PES, and second it permits us to obtain new kinetics and dynamics information for this reaction. Thus, the rate constants can be obtained at higher and lower temperatures, of interest in combustion and atmospheric chemistry, respectively, which are not available experimentally. The calculated rate constants show a small curvature of the Arrhenius plot, indicating the role of the tunneling factor in this reaction. This result seems logical given that a light particle (hydrogen atom) can easily tunnel through the barrier. The analysis of the reaction-path curvature, another dynamical feature, showed qualitatively that the C−F and C−Cl stretching vibrational excitations are expected in the products.

Finally, the agreement between our theoretical results and the experimental measurements (geometry, energy, and kinetics) lends confidence to the newly constructed PES, which can be used for trajectory calculations.

Acknowledgment. We are grateful to Prof. Donald G. Truhlar for providing a copy of the POLYRATE program, and to the Consejeria de Educación, Ciencia y Tecnología, Junta de Extremadura (Spain) (Project No. 2PR04A001) for partial financial support of this work.

References and Notes

(1) Espinosa-García, J. *J. Chem. Phys.* **1999**, *111*, 9330.
(2) Espinosa-García, J.; García-Bernáldez, J. C. *Phys. Chem. Chem. Phys.* **2000**, *2*, 2345.
(3) Corchado, J. C.; Truhlar, D. G.; Espinosa-García, J. *J. Chem. Phys.* **2000**, *112*, 9375.
(4) Espinosa-García, J.; Corchado, J. C. *J. Chem. Phys.* **2000**, *112*, 5731.
(5) Espinosa-García, J. *J. Chem. Phys.* **2002**, *116*, 10664.
(6) Espinosa-García, J. *J. Chem. Phys.* **2002**, *117*, 2076.
(7) Rangel, C.; Navarrete, M.; Espinosa-García, J. *J. Phys. Chem. A* **2005**, *109*, 1441.
(8) Rangel, C.; Espinosa-García, J. *J. Chem. Phys.* **2005**, *122*, 134315.
(9) Rangel, C.; Espinosa-García, J. *J. Phys. Chem. A* **2006**, *110*, 537.
(10) The reaction enthalpies were obtained from the following enthalpies of formation, ΔH_f°(298K), in kcal mol^{-1}: $CHClF_2$, −115.3±3.0 (ref 11); Cl, 28.99 (ref 11); ClH, −22.06 (ref 11); $CClF_2$, −64.30 (ref 12); CHF_2, −61.40 (ref 13); CHClF, −15.2 (ref 14); FCl, −12.0 (ref 11).
(11) In *JANAF Thermochemical Tables*, 3rd ed.; Chase, M. W., Davies, C. A., Jr., Downey, J. R., Frurip, D. J., McDonald, R. A., Syverud, A. N.; National Bureau of Standards: Washington, DC, 1985; Vol. 14.
(12) McMillen, D. F.; Golden, D. M. *Ann. Rev. Phys. Chem.* **1982**, *33*, 493.
(13) Leroy, G.; Dewispelaere, J. P.; Benkadour, H.; Riff, D.; Willante, C. *Bull. Soc. Chim. Belg.* **1994**, *103*, 367.
(14) Schwartz, M.; Peebles, L. R.; Berry, R. J.; Marshall, P. *J. Chem. Phys.* **2003**, *118*, 557.
(15) Jourdain, J. L.; Poulet, G.; Barassin, J.; Bras, G.; Combourieu, J. *Pollut. Atmos.* **1977**, *75*, 256.
(16) Tuazon, E. C.; Atkinson, R;.; Corchnoy, S. B. *Int. J. Chem. Kinet.* **1992**, *24*, 639.
(17) Sawerysyn, J. P.; Talhaoui, A.; Meriaux, B.; Devolder, P. *Chem. Phys. Lett.* **1992**, *198*, 197.
(18) Talhaoui, A.; Louis, F.; Meriaux, B.; Devolder, P.; Sawerysyn, J. P. *J. Phys. Chem.* **1996**, *100*, 2127.
(19) DeMore, W. B.; Sander, S. P.; Golden, D. M.; Hampson, R. F.; Kurylo, M. J.; Howard, C. J.; Ravishankara, A. R.; Kolb, C. J.; Molina, M. J. *Chemical Kinetic and Photochemical Data for Use in Stratospheric Modeling: Evaluation No. 11 of the NASA Panel for Data Evaluation*; JPL Publication 94-26; 1994.
(20) DeMore, W. B.; Sander, S. P.; Golden, D. M.; Hampson, R. F.; Kurylo, M. J.; Howard, C. J.; Ravishankara, A. R.; Kolb, C. E.; Molina, M. J. *Chemical Kinetics and Photochemical Data for Use in Stratospheric Modeling*; Evaluation Number 12, JPL Publication 97-4; 1997.
(21) Atkinson, R.; Baulch, D. L.; Cox, R. A.; Hampson, R. F., Jr.; Kerr, J. A.; Rossi, M. J.; Troe, J. *Evaluated Kinetic, Photochemical and Heterogeneous Data for Atmospheric Chemistry: Supplement V*; IUPAC: 1997.
(22) Atkinson, R.; Baulch, D. L.; Cox, R. A.; Crowley, J. N.; Hampson, R. F, Jr.; Kerr, J. A.; Rossi, M. J.; Troe, J. *Summary of Evaluated Kinetic and Photochemical Data for Atmospheric Chemistry*; IUPAC: 2001.
(23) Xiao, J-F.; Li, Z-S.; Ding, Y-H.; Liu, J-Y.; Huang, X-R.; Sun, C-C. *J. Phys. Chem. A* **2002**, *106*, 320.
(24) Li, Q. S.; Wang, C. Y. *Phys. Chem. Chem. Phys.* **2002**, *4*, 4386.
(25) Knyazev, V. D. *J. Phys. Chem. A* **2003**, *107*, 11082.
(26) Duchovic, R. J.; Hase, W. L.; Schlegel, H. B. *J. Phys. Chem.* **1984**, *88*, 1339.
(27) http://w3qf. unex. es/html/superficies. htm.
(28) Allison, T. C.; Truhlar, D. G.In *Modern Methods for Multidimensional Dynamics Computations in Chemistry*; Thomson, D. L., Ed.; World Scientific: Singapore, 1998.
(29) Chuang, Y-Y.; Truhlar, D. G. *J. Phys. Chem.* **1997**, *101*, 3808.
(30) Miller, W. H.; Handy, N. C.; Adams, J. E. *J. Chem. Phys.* **1980**, *72*, 99.
(31) Morokuma, K.; Kato, S. In *Potential Energy Surface and Dynamics Calculations*; Truhlar, D. G.; Plenum: New York, 1981; p 243.
(32) Kraka, E.; Dunning, T. H. In *Advances in Molecular Electronic Structure Theory*; JAI: New York, 1990; Vol. 1, p 129.
(33) Truhlar, D. G.; Isaacson, A. D.; Garrett, B. C. In *The Theory of Chemical Reactions*; Baer, M.; CRC: Boca Raton, FL, 1985; Vol. 4.
(34) Liu, Y-P.; Lynch, G. C.; Truong, T. N.; Liu, D-h.; Truhlar, D. G. *J. Am. Chem. Soc.* **1993**, *115*, 2408.
(35) Fernández-Ramos, A.; Truhlar, D. G. *J. Chem. Phys.* **2001**, *114*, 1491.
(36) Garrett, B. C.; Truhlar, D. G. *J. Chem. Phys.* **1982**, *76*, 1853.
(37) Corchado, J. C.; Chuang, Y-Y.; Fast, P. L.; Villa, J.; Hu, W-P.; Liu, Y-P.; Lynch, G. C.; Nguyen, K. A.; Jackels, C. F.; Melissas, V. S.; Lynch, B. J.; Rossi, I.; Coiti˜no, E. L.; Fernández-Ramos, A.; Steckler, R.; Garrett, B. C.; Isaacson, A. D.; Truhlar, D. G. *POLYRATE*, version 8.5.1; University of Minnesota: Minneapolis, MN, 2000.